Title
Structural Insights into the Dynamic Process of β2-Adrenergic Receptor Signaling

Journal
Cell, 161(5)

ISSN
0092-8674

Authors
Manglik, Aashish
Kim, Tae Hun
Masureel, Matthieu
et al.

Publication Date
2015-05-01

DOI
10.1016/j.cell.2015.04.043

Peer reviewed

HHS Public Access

Author manuscript

Cell. Author manuscript; available in PMC 2016 May 21.

Published in final edited form as:

Cell. 2015 May 21; 161(5): 1101–1111. doi:10.1016/j.cell.2015.04.043.

Structural insights into the dynamic process of β_2-adrenergic receptor signaling

Aashish Manglik[1,4], **Tae Hun Kim**[2,4], **Matthieu Masureel**[1], **Christian Altenbach**[3], **Zhongyu Yang**[3], **Daniel Hilger**[1], **Michael T. Lerch**[3], **Tong Sun Kobilka**[1], **Foon Sun Thian**[1], **Wayne L. Hubbell**[3,5], **R. Scott Prosser**[2,5], and **Brian K. Kobilka**[1,5]

[1]Department of Molecular and Cellular Physiology, Stanford University, Stanford, CA 94305, USA

[2]Department of Chemistry, University of Toronto, UTM, 3359 Mississauga Road North, Mississauga, Ontario, L5L 1C6, Canada

[3]Jules Stein Eye Institute and Department of Chemistry and Biochemistry, University of California, Los Angeles, CA 90095-7008, USA

SUMMARY

G protein-coupled receptors (GPCRs) transduce signals from the extracellular environment to intracellular proteins. To gain structural insight into the regulation of receptor cytoplasmic conformations by extracellular ligands during signaling, we examine the structural dynamics of the cytoplasmic domain of the β2-adrenergic receptor (β2AR) using ^{19}F-fluorine NMR and double electron-electron resonance spectroscopy. These studies show that unliganded and inverse-agonist-bound β2AR exists predominantly in two inactive conformations that exchange within hundreds of microseconds. Although agonists shift the equilibrium towards a conformation capable of engaging cytoplasmic G proteins, they do so incompletely, resulting in increased conformational heterogeneity and the coexistence of inactive, intermediate and active states. Complete transition to the active conformation requires subsequent interaction with a G-protein or an intracellular G protein mimetic. These studies demonstrate a loose allosteric coupling of the agonist-binding site and G protein-coupling interface that may generally be responsible for the complex signaling behavior observed for many GPCRs.

*Correspondence: kobilka@stanford.edu (B.K.K.).
[4]Co-first author
[5]Co-senior author

SUPPLEMENTAL INFORMATION

Supplemental information includes Extended Experimental Procedures, five figures, one table, and can be found with this article online.

AUTHOR CONTRIBUTIONS

A.M. designed NMR and DEER experiments, performed receptor purifications, and collected and analyzed DEER data. T.H.K. designed NMR experiments and collected and analyzed NMR data. M.M. purified receptor, performed DEER data collection, and analyzed DEER data. C.A., Z.Y., and M.T.L. collected and analyzed DEER data. D.H. assisted with DEER data analysis. T.S.K. and F.S.T. purified receptor for NMR studies. The manuscript was written by A.M., B.K.K., and R.S.P. W.L.H. supervised DEER data collection and analysis, R.S.P. supervised NMR data collection and analysis, and B.K.K. supervised the overall project.

INTRODUCTION

G protein-coupled receptor signaling relies on allosteric coupling between the extracellular facing ligand binding pocket and the cytoplasmic domain of the receptor. Ligands may activate a signaling pathway (agonists), inhibit the basal level of signaling (inverse agonists), or bind but not perturb signaling (neutral antagonists), all by changing the conformational ensemble of a GPCR. Recent X-ray crystal structures of the β_2AR have provided high-resolution insight into two conformations associated with GPCR function: an inactive, inverse agonist-bound state and the active state in complex with an agonist and the G protein G_s (Cherezov et al., 2007; Rasmussen et al., 2011a; Rasmussen et al., 2007; Rasmussen et al., 2011b; Rosenbaum et al., 2007). These structures reveal how subtle changes in the ligand-binding pocket translate into a 14 Å outward displacement of transmembrane 6 (TM6) in the cytoplasmic domain of the receptor (Figure 1A)(Trzaskowski et al., 2012).

Proteins display a range of motions associated with function, from pico- to nanosecond timescale amino acid side chain reorientations to inter-domain motions that may happen on the millisecond to second timescale (Baldwin and Kay, 2009; Henzler-Wildman and Kern, 2007; Sekhar and Kay, 2013). Although such protein dynamics are likely important for the signaling versatility and allosteric regulation of GPCRs, the dynamic properties of GPCRs remain poorly understood. Crystallography typically captures the lowest energy states within an ensemble of conformations. Other methods are therefore required to characterize transiently populated conformations as well as the transitions between different conformations. Using NMR spectroscopy of $^{13}CH_3$-ε-methionines, we recently observed significant conformational heterogeneity in the transmembrane core of β_2AR while bound to agonist and inverse agonist, as well as evidence of conformations not observed in crystal structures (Kofuku et al., 2012; Nygaard et al., 2013). Here, we extend these studies by assessing β_2AR conformational dynamics in the cytoplasmic, G protein-coupling domain of the receptor. We use ^{19}F NMR spectroscopy of fluorine labeled β_2AR to identify representative states and exchange rates between these states as a function of ligand efficacy. To provide a structural framework for this conformational heterogeneity, we utilize pulsed electron paramagnetic resonance spectroscopy (double electron-electron resonance or DEER) of nitroxide spin labeled β_2AR.

RESULTS

Monitoring β_2AR structure and dynamics with NMR and DEER spectroscopy

For ^{19}F-NMR studies, we site-specifically labeled a minimal cysteine version of β_2AR with a trifluoroacetanilide probe at Cys265, an endogenous residue located at the cytoplasmic end of TM6 (Figure 1B and Figure S1A) (Jensen et al., 2000). The resulting ^{19}F-NMR spectrum displays peaks at different chemical shifts that reflect the unique environments of the trifluoromethyl probe at Cys265 associated with specific conformations of TM6 and neighboring TM3, TM5 and TM7. Each peak defines a given conformation or state. In one dimensional NMR, the area associated with a peak is in direct proportion to the population of that conformer. The line width reflects subtle conformational heterogeneity or exchange

dynamics between states, which can be distinguished by additional Carr-Purcell-Meiboom-Gill (CPMG) relaxation dispersion measurements (Meiboom and Gill, 1958). Thus, NMR spectra reveal conformational heterogeneity in and around TM6, either as peak broadening or as multiple peaks with different chemical shifts. To aid in the visualization of ^{19}F-NMR spectra, we subtract a peak originating from another labeled site on the β_2AR that does not change upon addition of ligands. The original spectrum originating from Cys265 and the subtracted constant peak are shown in Figure S1B and S1C.

To provide a structural framework for the conformational heterogeneity observed in ^{19}F-NMR spectra, we utilized DEER spectroscopy, which can measure distance distributions between two domains on a protein. For DEER spectroscopy, β_2AR was site-specifically labeled with nitroxide probes at L266C in TM6 and N148C in TM4 (Figure 1C and Figure S1A, S1D, and S1E) and the DEER data were analyzed to provide inter-nitroxide distance distributions using established methods (Figure S2). Finally, we performed two additional ^{19}F-NMR relaxation experiments designed to examine the kinetics of conformational changes: CPMG relaxation dispersion experiments for fast microsecond to millisecond transitions, and “hole burning” saturation-transfer experiments for slow transitions occurring on the 10–500 millisecond timescale (Forsen and Hoffman, 1963). Studies were performed with protein purified by ligand affinity chromatography to ensure that all spectroscopic data reflects functional states of the β_2AR (Kobilka, 1995).

We acquired spectra for β_2AR bound to saturating concentrations of four ligands: carazolol, an ultra high-affinity (32 pM) partial inverse agonist (Rasmussen et al., 2007); ICI-118,551, a high-affinity (550 pM) full inverse agonist (Baker, 2005); isoproterenol, a low-affinity (229 nM) full agonist that is an analog of the endogenous hormone adrenaline; and BI167107, an ultra-high affinity full agonist (84 pM)(Rasmussen et al., 2011a). Additionally, we acquired spectra for β_2AR bound to either agonist in the presence of the G protein mimetic Nb80. In total, NMR and DEER spectroscopy provide evidence for at least four distinct β_2AR states, which we label as S1, S2, S3, and S4 for the purpose of discussion (Figure 1D, top panel). While it is possible that the states identified by NMR and DEER spectroscopy are distinct and non-overlapping, the high level of agreement observed for equilibrium populations and their response to ligands strongly suggest that both techniques resolve similar conformations of the β_2AR. After assigning these states to specific structural conformations of the β_2AR, we illustrate insights into receptor function with energy landscape diagrams that change in presence of inverse agonists, agonists, and Nb80 (Figure 1D). Although the energy diagram illustrations likely over-simplify the complexity of β_2AR dynamics, they show the key role that structural dynamics plays in GPCR function. Furthermore, the results suggest a marked difference in the conformational landscape of β_2AR as compared to the light sensing GPCR rhodopsin. These differences in energetics may explain dissimilarities in signaling behavior between rhodopsin, which evolved for rapid and highly efficient detection of a photon, and hormone activated GPCRs like the β_2AR, which evolved to have more complex signaling and regulatory behavior.

Dynamics of inactive states

To provide a structural reference for NMR and DEER studies, we will first present results of experiments done under conditions used to obtain inactive and active state crystal structures. Carazolol is an ultra-high affinity partial inverse agonist that reduces basal G_s coupling activity (Rasmussen et al., 2007). DEER spectroscopy revealed a broad distance distribution between TM6 and TM4 (Figure 2A). Modeling of the nitroxide spin labels in the carazolol bound X-ray crystal structure of β_2AR (PDB ID: 4GBR)(Zou et al., 2012) and simulation of the expected distance distribution (see Methods) showed substantial overlap with one of the populations observed in the DEER derived distance distribution (Figure 2A and 2B). While the conformation of TM6 is similar in all inactive state crystal structures of the β_2AR, structural heterogeneity of TM6 in the inactive state has previously been observed in crystal structures of the β_1AR (Moukhametzianov et al., 2011), where one of two TM6 conformations resulted from different states of a highly conserved interaction between the DRY motif within TM3 and E285$^{6.30}$, termed the ionic lock. Although crystal structures of antagonist bound β_2AR consistently show a broken ionic lock, molecular dynamics simulations indicate that the receptor transitions frequently between the two conformations (Dror et al., 2009). In order to assess the theoretical DEER distance distribution for β_2AR in the ionic lock, we modeled the nitroxide labels onto the X-ray crystal structure of β_1AR with an intact ionic lock (PDB: 2YCW, Chain A) at the same positions used for DEER studies of the β_2AR (Figure 2A and 2C) and simulated the inter-nitroxide distance distribution. This simulated distribution for β_1AR with an intact ionic lock overlaps one of the conformations experimentally observed for β_2AR. This ensemble with shorter distances may thus represent a population of the β_2AR with an intact ionic lock. We describe the inactive conformation with the ionic lock intact as S1 and the conformation with the ionic lock broken as S2. We observe a smaller population having shorter distances between nitroxide probes (28–33Å). These may reflect additional, less populated conformational states and/or different rotamers of probes on the S1 conformation.

In agreement with the structural heterogeneity observed in DEER experiments, ^{19}F-NMR spectra show a broad line shape. Due to the slow dissociation rate of carazolol ($t_{1/2}$ of dissociation = 30.4 hours)(Rosenbaum et al., 2007) compared to the timescale of the NMR experiment, ligand association and dissociation kinetics do not contribute to the observed structural heterogeneity and dynamics. In accord with molecular dynamics simulations, we observed the presence of high microsecond receptor exchange dynamics (exchange rate (k_{ex}) = 6200 ± 830 s $^{-1}$) for carazolol-bound β_2AR in CPMG relaxation dispersion experiments (Figure 3A, inset). As a result of the exchange rate between the two ionic lock states, their unique chemical shifts are not observed in the spectra but are represented as a weighted average centered at −60.85 ppm due to classic exchange broadening and coalescence. However, knowing the exchange rate and assuming two states as suggested by the DEER distance distributions, it is possible to simulate the NMR lineshapes and chemical shifts for each of these states as they would appear in the absence of exchange (see Extended Experimental Methods). The resulting simulated exchange-free spectra identify two states that likely correspond to the ionic lock states S1 and S2 (Figure 3A and Figure S3B). We assign the peak at −60.50 ppm to S1 (ionic lock intact) since more buried fluorine reporters are typically observed to be more downfield. Moreover, the linewidth of S2 (−61.30 ppm) in

the absence of exchange is predicted to be broader based on the global lineshape simulations, hinting at greater heterogeneity in the ionic lock disrupted inactive state. For carazolol-bound β_2AR, both states are populated nearly equally, which is consistent with the results observed by DEER spectroscopy for the S1 and S2 states. Using these equilibrium populations for S1 and S2 with the exchange kinetics from the CPMG experiments, the calculated lifetime of the S1 and S2 states is 325 ± 44 μs (Figure 3C). Together these results show that the inverse agonist carazolol does not fully stabilize TM6 in a single inactive conformation. In Figure 1D, we represent the two states observed for carazolol-bound β_2AR as two energy wells of similar depth separated by a shallow energy barrier that allows the fast exchange between the two inactive conformations.

Dynamics of fully active state

Activation of the β_2AR results in TM6 movement that creates a receptor-binding site for intracellular effector and regulatory proteins. This change was observed in crystal structures of β_2AR bound to BI167107 and either G_s or Nb80 (Rasmussen et al., 2011a; Rasmussen et al., 2011b). We utilized Nb80 as a G protein surrogate in NMR and DEER experiments for two reasons (Figure 2D and Figure 3B). First, generating homogeneously prepared β_2AR bound to Nb80 is significantly simpler as compared to G_s, as Nb80 binding does not depend on biochemically labile nucleotides. Secondly, Nb80 is significantly smaller than G_s (14 kDa versus 85 kDa), and this smaller size allowed us to generate ^{19}F-NMR spectra of fully activated receptor with greater resolution due to longer transverse relaxation times. The ^{19}F-NMR spectrum of the β_2AR-BI167107-Nb80 complex shows a large change from the unliganded state, with the appearance of a new peak (Figure 3B). The upfield chemical shift of −61.59 ppm observed for β_2AR bound to Nb80 is consistent with greater solvent exposure of the cytoplasmic side of TM6 upon receptor activation. Additionally, the decreased peak linewidth is consistent with a single receptor conformation while bound to Nb80. Additionally, CPMG experiments revealed no evidence of millisecond timescale exchange dynamics (Figure 3B, inset).

Using DEER spectroscopy, we confirmed that the change in the ^{19}F-NMR spectrum occurs due to receptor activation (Figure 2D). The distance distribution shows a single conformation centered around 50 Å, consistent with the outward displacement of TM6 observed in the crystal structure of the β_2AR-BI167107-Nb80 complex. Simulation of the inter-nitroxide distance distribution for spin labels modeled in the β_2AR-BI167107-Nb80 crystal structure (PDB ID: 3P0G) yielded good agreement with the observed DEER distance distribution (Figure 2D and 2E). Binding of a high-affinity agonist and an intracellular G protein mimetic, therefore, fully stabilizes β_2AR in the conformation observed by X-ray crystallography. The absence of exchange dynamics in ^{19}F-NMR CPMG experiments (Figure 3B, inset) suggests that this activated conformation in the presence of BI167107 and Nb80 is a relatively stable, low-energy conformation. In Figure 1D, we depict the corresponding free energy landscape, resulting from binding of agonist and Nb80, as being dominated by a single energy well, with a large energy barrier towards alternative conformations of the β_2AR. We refer to the fully active conformation with both agonist and Nb80 bound as S4. As the structure of Nb80-bound β_2AR is highly similar to that of the

β_2AR-G_s complex, the S4 state likely also represents the G protein-coupled state of the receptor.

Structural Insights into Basal Activity

Most GPCRs, including the β_2AR, exhibit some degree of basal activity suggesting that they are able to activate G proteins in the absence of agonist. The structural basis for basal activity isn't known, but may be due to the dynamic and flexible nature of the β_2AR such that a small fraction of receptor existing in an active state is capable of coupling to G_s. Inverse agonists like carazolol and ICI-118,551 would be expected to destabilize active states, either by reducing their equilibrium population or decreasing the lifetime of states on the pathway to activation. Surprisingly, there is little difference in the steady-state DEER and NMR data between unliganded receptor and β_2AR bound to carazolol or ICI-118,551 (Figure 4A, 4B and Figure S4A, S4B). The relative populations of S1 and S2 as determined by lineshape simulations are similar for unliganded and inverse agonist-bound receptor (Figure 4C). Notably, we do not reliably observe a peak corresponding to the active state in either DEER or NMR experiments of unliganded β_2AR, likely because such a transiently populated conformation is outside the current detection limit of these experiments. However, CPMG experiments show that the rate of interconversion between the S1 and S2 states is reduced by approximately half for unliganded receptor as compared with either carazolol-bound or ICI-118,551-bound receptor (Figure 4B inset and Figure S4B). The more rapid exchange between S1 and S2 in carazolol and ICI-118,551-bound receptor is illustrated in the energy landscape as a lower energy barrier between these two states (Figure 1D). This lower interconversion rate for unliganded receptor also results in an increased lifetime of both the S1 and S2 states, with a calculated value of 700 ± 137 μs (Figure 3C).

Agonists alone do not fully stabilize an active state

Although it is well established that agonists increase GPCR signaling by inducing a change in receptor conformation and ultimately leading to G protein coupling, the mechanism associated with this allosteric process remains poorly understood. Crystal structures of β_2AR in a fully active conformation have relied on the presence of a protein bound to the intracellular surface to stabilize the active state. As a result, the degree of conformational changes induced by agonists alone remains poorly defined. In the absence of a stabilizing interaction with Nb80 or G_s, the β_2AR bound to a covalent agonist crystallized in an inactive conformation (Rosenbaum et al., 2011). Additionally, molecular dynamics simulations of active, agonist-bound β_2AR in the absence of Nb80 or G_s demonstrate a rapid transition of the receptor to the inactive state (Rosenbaum et al., 2011). These results, together with previous NMR studies (Nygaard et al., 2013), suggest that the active conformation is not the lowest energy state for agonist-bound receptor. Here, we explore the effect of agonists on the structure of the cytoplasmic domain of the β_2AR in the absence of constraints imposed by a crystal lattice.

To determine the effect of agonists on β_2AR structure and dynamics we examined two full agonists: isoproterenol (760 nM), a catecholamine related to adrenaline, and BI167107 (84 pM). In the case of isoproterenol, association and dissociation kinetics are rapid (seconds to minutes) and may contribute to receptor dynamics; however, the dissociation kinetics of

BI167107 are very slow ($t_{1/2}$ = 30 hours)(Rasmussen et al., 2011a) and this agonist will remain bound for the duration of the spectroscopic studies.

We first assessed the ability of the lower affinity full agonist isoproterenol to induce conformational changes in the β_2AR. Surprisingly, DEER experiments revealed that even in the presence of a saturating concentration (2.5× molar excess, 0.5 mM) of a full agonist, most of the receptor remained in an inactive conformation with approximately 20% in a conformation similar to the fully active β_2AR bound to BI167107 and Nb80 (Figure 5A). Isoproterenol also appears to increase the fraction of receptor populating a conformation consistent with a broken ionic lock when compared with unliganded and inverse agonist-bound receptor. To determine if the inactive-state peaks represent non-functional receptor, we added Nb80 and observed that most of the protein transitions to an active state (Figure 5A). NMR studies revealed a more complex set of conformations associated with agonists, perhaps due to the sensitivity of the ^{19}F-NMR probe to local conformation. We observe a new upfield peak in the ^{19}F-NMR spectrum (Figure 5B) in the presence of saturating concentrations of isoproterenol. This new peak, labeled S3, has a chemical shift of −61.47 ppm, which is similar but not identical to the S4 state (−61.59 ppm) observed for β_2AR bound to BI167107 and Nb80 (Figure 3B). Addition of Nb80 to isoproterenol-bound β_2AR results in a predominant peak between S3 and S4 at −61.51 ppm (Figure 5B). Although Nb80 was added in 2.5× molar excess, the fast dissociation/association kinetics of isoproterenol may hinder complete stabilization of the S4 state. The resulting conformational heterogeneity is consistent with the increased peak linewidth observed for β_2AR bound to isoproterenol and Nb80 as compared to BI167107 and Nb80 (144 Hz and 114 Hz, respectively) as well as the small fraction of inactive receptor observed in the DEER distance distribution. Given the sensitivity of the ^{19}F-NMR probe, we posit that the S3 peak represents an on-pathway intermediate towards the fully activated S4 conformation, which is adopted upon complete stabilization of the active state. In the experimental conditions presented here, this occurs only upon binding of a slowly dissociating agonist and Nb80. The fact that we cannot distinguish S3 from S4 by DEER spectroscopy may be due to limitations in sensitivity of this method at distances in the range of 50 Å. It is also possible that different conformations result in similar TM6-TM4 distances.

Based on the area under the S3 peak for isoproterenol bound β_2AR, this state represents approximately 15% of the total receptor population and is consistent with the fraction of receptor in the active-like state observed in DEER studies. Additionally, we performed lineshape simulations of the major peak arising from S1 and S2 states using estimates of receptor exchange kinetics derived from CPMG experiments (Figure 5C, 5D and Figure S5A). Such analysis shows that isoproterenol increases the fraction of β_2AR in the S2 state with a broken ionic lock, which is consistent with the proportions observed in DEER studies. Notably, due to the difference in population observed for S1 and S2 for isoproterenol-bound receptor, the calculated lifetimes differ for each state (Figure 3C). The S1 lifetime is 394 ± 55 μs, which is similar to that observed for carazolol-bound receptor. On the other hand, the lifetime of the S2 state is 756 ± 105 μs, similar to that for unliganded receptor. These observed differences in lifetimes of the S1 and S2 states between agonist, inverse agonist, and unliganded receptor are shown in Figure 3C.

To determine if the failure of isoproterenol to fully stabilize the active state is due to dissociation/association kinetics, we examined the response to the ultra high-affinity agonist BI167107. In both ^{19}F-NMR and DEER experiments, we observe substantially more of the S3 conformation of β_2AR (Figure 5E and 5F). However, even bound to this high affinity agonist, approximately 40–60% of the receptor is in conformations comprised of the inactive S1 and S2 states. As noted above, due to the very slow dissociation kinetics, it is unlikely that this observed conformational heterogeneity results from β_2AR molecules not bound to BI167107. The reduced signal representing S1 and S2 does not allow accurate measurement of relaxation dispersion by CPMG experiments. However, we observed slow exchange between active (S3) and inactive (S1 and S2) conformations in ^{19}F-NMR saturation transfer experiments. Saturation of the ^{19}F-NMR peak originating from the inactive state S1 led to a decrease in signal of the peak originating from the active intermediate S3, suggesting that inactive and active conformations exchange on a slow timescale (Figure 5G and 5H). Through control experiments, which allowed us to identify the extent of off-resonant saturation (Figure 5H and Figure S5C), the exchange resulting from saturating the inactive ensemble is consistent with the lifetime of the S3 state to be 660 ms. The kinetics of these transitions is faster than our previous fluorescence studies examining the activation of purified β_2AR by isoproterenol (Swaminath et al., 2004). In those experiments, the change in fluorescence associated with receptor activation occurs in two phases, with $t_{1/2}$ values of 2.5 s and 150 s. While these experiments highlighted the slow transition associated with receptor activation, the studies were done under non-steady state conditions where ligand binding and unbinding as well as receptor conformational changes contribute to the change in fluorescence. In the NMR kinetics experiment presented in Figure 5H, the receptor is at equilibrium between inactive and active states, and the agonist BI167107 has such exceptionally slow binding/unbinding kinetics that they do not contribute to the observed rate of transitions between inactive and active states. As such, the saturation transfer experiment here directly shows a high-energy barrier between the inactive and S3 states that may be responsible for the slower transition to the active state observed for the β_2AR and other GPCRs as compared to rhodopsin (Lohse et al., 2014).

DISCUSSION

Taken together, the spectroscopic results for β_2AR bound to BI167107 and isoproterenol suggest that agonists do not fully stabilize the active conformation of the receptor at the cytoplasmic domain. Furthermore, in each case, agonist-bound β_2AR is highly dynamic and interconverts between inactive, intermediate, and active conformations with varying timescales. In Figure 1D, we illustrate the effects of BI167107 and isoproterenol on β_2AR. BI167107 induces a greater decrease in energy of the active-like state S3. Isoproterenol, on the other hand, induces a small decrease in the energy of both the S2 and S3 states. Based upon their unique ^{19}F NMR chemical shifts, we distinguish the active intermediate state S3 stabilized by isoproterenol or BI167107 alone as being distinct from S4, the fully active state stabilized only in the presence of a slowly dissociating agonist and the G protein mimetic Nb80. It should be noted that we do not observe a difference between S3 and S4 in DEER studies. This may reflect the limits of spatial resolution of DEER spectroscopy, or the fact that S3 and S4 have the same maximum distance, but differ in the conformation of other TM

segments that are near C265 such as TM5 and TM7. Nevertheless, the distinction between S3 and S4 is supported by NMR experiments examining the dynamics of transmembrane $^{13}CH_3$-ε-methionines that revealed the inability of BI167107 to stabilize the transmembrane core of β_2AR in an active conformation in the absence of Nb80 (Nygaard et al., 2013). Taken together, these spectroscopic results suggest that the conformation of the ligand binding pocket and the cytoplasmic domain of β_2AR are not tightly allosterically coupled. This “loose allosteric” regulation has previously been proposed based on long timescale molecular dynamics simulations where agonist-bound β_2AR in an active conformation rapidly transitions to the inactive state, but without a high degree of correlation in conformation between the cytoplasmic domain and the ligand binding pocket (Dror et al., 2011).

The regulation of β_2AR by agonists and inverse agonists demonstrated here stands in contrast to what has been observed for the light sensitive transducer rhodopsin, the GPCR that has been most extensively characterized by biophysical methods (Figure 6). Similar to the experiments presented here for the β_2AR, conformational changes in rhodopsin have previously been studied in a detergent environment. While the dynamic properties of both rhodopsin and β_2AR are predicted to be influenced by the lipid environment of a cellular membrane, both receptors are functional in dodecyl-maltoside. Using this detergent in the DEER experiments presented here allows us to compare the intrinsic dynamics of the β_2AR with previously published studies on rhodopsin. In the presence of the covalently attached inverse agonist 11-*cis*-retinal, EPR and NMR experiments show that TM6 of rhodopsin primarily adopts a single inactive conformation that is partly stabilized by the intracellular ionic lock (Klein-Seetharaman et al., 1999; Knierim et al., 2007); Smith (2010). In contrast, carazolol-bound β_2AR is more dynamic in the inactive state, with rapid transitions between conformations likely representing different states of the β_2AR ionic lock.

Like β_2AR, rhodopsin activation is also associated with an outward displacement of TM6 (Altenbach et al., 2008; Choe et al., 2011; Standfuss et al., 2011). Crystallographic and spectroscopic studies have illuminated how light-induced activation of rhodopsin results in multiple conformations of the receptor, including some states that exist for a very short period of time (Okada et al., 2001). Isomerization of 11-*cis*-retinal to the agonist all-*trans*-retinal results in conformational heterogeneity around the retinal-binding pocket, with a rapid equilibrium reached between Meta I and Meta II states. Elegant spectroscopic and crystallographic studies have utilized pH, ionic strength, temperature, and reconstitution into defined lipid environments to stabilize and characterize these different conformations (Delange et al., 1997; Gibson and Brown, 1993; Parkes and Liebman, 1984). In experiments performed in detergent at neutral pH, however, light-activated rhodopsin completely populates the Meta IIb conformation, which is characterized by an outward displacement of TM6 (Figure 6B)(Altenbach et al., 2008; Arnis and Hofmann, 1993; Knierim et al., 2007). The allosteric coupling between the ligand binding pocket and TM6 conformation, however, is significantly less rigid for the β_2AR in the experiments presented here. Agonist-bound β_2AR is considerably more dynamic, and a significant fraction of agonist- bound receptor adopts an inactive (S2) or active-like intermediate (S3) conformation (Figure 6A). Transition to the active conformation observed in the structure of β_2AR coupled to G_s

therefore requires the heterotrimeric G protein in addition to the agonist. This is likely to involve a multistep process where G_s initially engages S3 or a similar state and arrives at the fully active conformation through one or more yet uncharacterized conformational intermediates.

The structural basis of basal activity and inverse agonism is not known. The spectroscopy studies presented here do not reliably detect a population in the active state for the unliganded receptor. However, given the relatively small population of active intermediate S3 observed in the presence of the full agonist isoproterenol, it is possible that a small amount of S3 that is outside the detection limit of these spectroscopic experiments could result in substantial activation of G_s. In addition to the population of active conformations, receptor activation and ligand efficacy may also be governed by the lifetime of inactive states. While the populations of S1 and S2 are not different for unliganded and carazolol-bound receptor (Figure 1D), we do observe a difference in the exchange rate between these states by CPMG experiments. The more rapid exchange observed in the presence of carazolol and ICI-118,551 is associated with a shorter lifetime of both S1 and S2 (Figure 1D and 3C). In particular, we speculate that the lifetime of S2 (ionic lock broken) is relevant to activation. Conversion between the inactive S2 and active-like S3 states involves a significant energy barrier and a large rearrangement of receptor topology. As such, this conversion process is likely highly sensitive to the lifetime of the ionic lock broken (S2) state. Inverse agonists may reduce the lifetime of S2 below the characteristic timescale required for the conversion from S2 to S3, thereby curtailing receptor activation. Therefore, inverse agonist suppression of basal activity may result from both a decrease in receptor population of intermediate active states and a decreased lifetime of states on the path to activation.

In conclusion, we demonstrate here a loose allosteric regulation of the cytoplasmic, G protein-coupling domain of the β_2AR. For many GPCRs, similar loose allostery may be responsible for the ability of agonist-bound receptors to regulate multiple intracellular signaling pathways through direct interactions with different signaling and regulatory proteins. While the spectroscopy studies presented here only examine one dimension of activation, namely the outward movement of TM6, they highlight the complexity of receptor conformation. More generally, the studies presented here highlight the key role that protein dynamics likely play in the signaling properties of GPCRs. Further characterization of such dynamics will be required to better understand signal transduction and to leverage GPCR structural biology for drug design.

EXPERIMENTAL PROCEDURES

β_2AR expression, purification, and sample preparation

Site-specific labeling of full-length human β_2AR utilized a minimal cysteine version of the receptor with mutations C77V, C327S, C378A and C406A and with normal ligand binding properties as assessed by the affinities of the antagonist ^{3}H-dihydroalprenolol, the inverse agonist ICI-118,551 and the agonist isoproterenol (Figure S1A and Table S1). Sites of interest were mutated to cysteine on top of this minimal cysteine β_2AR variant (termed β_2AR-Δ4) and expressed in *Sf9* insect cells using baculoviruses encoding receptor

constructs. More details of the construct design are provided in Extended Experimental Procedures. After infection and expression of β_2AR, cells were lysed and β_2AR was extracted using the detergent dodecylmaltoside. Anti-FLAG antibody chromatography was used to purify receptor followed by labeling with either ^{19}F-BTFA at the endogenous residue C265 for ^{19}F-NMR experiments or IA-PROXYL at residues L266C and N148C for DEER experiments. Labeled β_2AR was further purified by alprenolol-sepharose ligand affinity chromatography to isolate only functional receptor molecules and concentrated to 200–300 μM. To assess the conformation of unliganded receptor, we incorporated a wash with the low-affinity antagonist atenolol to generate homogenously ligand-depleted samples. For ^{19}F-NMR experiments, the detergent was gradually exchanged to lauryl maltose neopentyl glycol (MNG-3, Anatrace). Prior to collecting spectroscopic data, the receptor was incubated for at least one hour with a 2.5× molar excess of ligands or Nb80. Nb80 was purified as previously described (Rasmussen 2011a).

^{19}F-NMR spectroscopy

NMR spectra were acquired at 25°C on a 600 MHz Vari an Inova spectrometer and a 500 MHz Varian Unity spectrometer equipped with a cryogenic probe capable of ^{19}F NMR (600 MHz) or a room temperature ^{19}F probe (500 MHz). Free induction decay (FID) signals were acquired with a π/2 pulse length of 18 μs, a repetition time of 1.5 s, and an acquisition time of 0.25 s. The FID, which consisted of 4,500 complex points, was linear predicted to 16,000 points, backward linear predicated 3 points, and apodized with 20 Hz Lorentzian filter. All spectral processing was performed using Mnova 9.0.0 (Mestrelab Research) and illustrated spectra are normalized to the integral under the peak arising from Cys265. CPMG relaxation dispersion spectra were fit to a two-state exchange model with Chemex (Shi and Kay, 2014). Errors in $R_{2,eff}$ were estimated by the spectral noise and variation in spectra between experiments from identically prepared samples. The fitting program, ChemEx, uses this estimate of $R_{2,eff}$ error when calculating the reduced X^2 values and the errors in k_{ex} are extracted from the covariance associated with this parameter. Saturation transfer experiments done for β_2AR bound to BI167107 utilized continuous-wave irradiation of the S1 and S2 states 420 Hz downfield of the S3 state. The saturation pulse duration ranged from 25–1000 ms. To control for direct saturation of the S3 peak, a similar experiment was performed with irradiation 420 Hz upfield of the S3 state. The lifetime of S3, τ_3, was fit using measured estimates of T_1 for the peaks of interest, and accounting for direct off-resonance saturation effects as described elsewhere (Spoerner et al., 2010). Lineshape simulations of NMR peaks were performed using a global fit of all spectra and the exchange rate (k_{ex}) determined from CPMG experiments using the program WinDNMR (Reich, 1995). Further details about the specific parameters used for fitting can be found in the Extended Experimental Methods.

DEER spectroscopy and nitroxide label simulation

For DEER spectroscopy, glycerol was added to a final concentration of 20% (v/v) immediately prior to data collection. Samples were flash frozen in liquid nitrogen and dipolar evolution data were acquired at Q-band on a Bruker ELEXSYS 580 at 80 K. DEER data were analyzed using the program LongDistances, which was written in LabVIEW by C.A. and is available for download at http://www.biochemistry.ucla.edu/biochem/Faculty/

Hubbell/. The dipolar evolution for each sample was fit using a model-free analysis similar to the widely used Tikhonov regularization. The background subtracted dipolar data, their fits, and the resulting distance distributions are shown in Figure S2. All data was plotted using GraphPad Prism 6 after normalizing the area under the distance probability distribution. To simulate DEER distance distributions for existing crystal structures, the IA-PROXYL spin label was built onto existing crystal structures using the program MTSSLWizard (Hagelueken et al., 2012), and the program was used to generate an ensemble of rotamers which avoid steric clashes with the static protein structure. This was followed by a computation of the distance distribution between labeled sites. Distances between the resulting spin label rotamers were plotted in GraphPad Prism 6 and normalized to have the same area under the curve as the experimentally derived spectra.

As changes in distance can originate from changes in the spin label rotamer, we collected CW-EPR spectra of IA-PROXYL labeled β_2AR-Δ5-L266C and β_2AR-Δ5-N148C to determine whether the most extreme changes in the DEER data were correlated to changes in nitroxide spin label conformation (Figure S1D). We observed minimal or no changes upon addition of carazolol, BI167107, and BI167107+Nb80, indicating that the observed changes in distance are primarily due to rigid body motions between TM6 and TM4. DEER spectra for singly labeled β_2AR-Δ5-L266C and β_2AR-Δ5-N148C demonstrated the absence of any preferred distance above background (Figure S1E), indicating that the observed distance distributions for the doubly labeled β_2AR-Δ5-L266C-N148C construct correspond only to the distance between L266C and N148C.

Supplementary Material

Refer to Web version on PubMed Central for supplementary material.

ACKNOWLEDGEMENTS

This work was supported by American Heart Association Award 12PRE8120001 (A.M.) and 15POST22700020 (M.M.), by the Natural Sciences and Engineering Research Council of Canada under a Discovery Award (261980) and Research Accelerator Award (R.S.P.), and by the National Institutes of Health under award numbers R01EY005216 and P30EY00331 (W.L.H.), R01GM083118 and R01NS028571 (B.K.K.). We would also like to acknowledge support from the Jules Stein Professor endowment (W.L.H.). T.H.K. was supported by the Canadian Institutes of Health Research Training Program in Protein Folding and Interaction Dynamics. D.H. was supported by the German Academic Exchange Service (DAAD). M.M. was supported by a Hoover Foundation Brussels Fellowship from the Belgian American Educational Foundation.

REFERENCES

Altenbach C, Kusnetzow AK, Ernst OP, Hofmann KP, Hubbell WL. High-resolution distance mapping in rhodopsin reveals the pattern of helix movement due to activation. Proceedings of the National Academy of Sciences of the United States of America. 2008; 105:7439–7444. [PubMed: 18490656]

Arnis S, Hofmann KP. Two different forms of metarhodopsin II: Schiff base deprotonation precedes proton uptake and signaling state. Proceedings of the National Academy of Sciences of the United States of America. 1993; 90:7849–7853. [PubMed: 8356093]

Baker JG. The selectivity of beta-adrenoceptor antagonists at the human beta1, beta2 and beta3 adrenoceptors. British journal of pharmacology. 2005; 144:317–322. [PubMed: 15655528]

Baldwin AJ, Kay LE. NMR spectroscopy brings invisible protein states into focus. Nature chemical biology. 2009; 5:808–814.

Cherezov V, Rosenbaum DM, Hanson MA, Rasmussen SG, Thian FS, Kobilka TS, Choi HJ, Kuhn P, Weis WI, Kobilka BK, et al. High-resolution crystal structure of an engineered human beta2-adrenergic G protein-coupled receptor. Science. 2007; 318:1258–1265. [PubMed: 17962520]

Choe HW, Kim YJ, Park JH, Morizumi T, Pai EF, Krauss N, Hofmann KP, Scheerer P, Ernst OP. Crystal structure of metarhodopsin II. Nature. 2011; 471:651–655. [PubMed: 21389988]

Delange F, Merkx M, Bovee-Geurts PH, Pistorius AM, Degrip WJ. Modulation of the metarhodopsin I/metarhodopsin II equilibrium of bovine rhodopsin by ionic strength--evidence for a surface-charge effect. European journal of biochemistry / FEBS. 1997; 243:174–180. [PubMed: 9030737]

Dror RO, Arlow DH, Borhani DW, Jensen MO, Piana S, Shaw DE. Identification of two distinct inactive conformations of the beta2- adrenergic receptor reconciles structural and biochemical observations. Proceedings of the National Academy of Sciences of the United States of America. 2009; 106:4689–4694. [PubMed: 19258456]

Dror RO, Arlow DH, Maragakis P, Mildorf TJ, Pan AC, Xu H, Borhani DW, Shaw DE. Activation mechanism of the beta2-adrenergic receptor. Proceedings of the National Academy of Sciences of the United States of America. 2011; 108:18684–18689. [PubMed: 22031696]

Forsen S, Hoffman RA. Study of Moderately Rapid Chemical Exchange Reactions by Means of Nuclear Magnetic Double Resonance. J Chem Phys. 1963; 39 2892-&.

Gibson NJ, Brown MF. Lipid headgroup and acyl chain composition modulate the MI-MII equilibrium of rhodopsin in recombinant membranes. Biochemistry. 1993; 32:2438–2454. [PubMed: 8443184]

Hagelueken G, Ward R, Naismith JH, Schiemann O. MtsslWizard: In Silico Spin-Labeling and Generation of Distance Distributions in PyMOL. Applied magnetic resonance. 2012; 42:377–391. [PubMed: 22448103]

Henzler-Wildman K, Kern D. Dynamic personalities of proteins. Nature. 2007; 450:964–972. [PubMed: 18075575]

Jensen AD, Guarnieri F, Rasmussen SG, Asmar F, Ballesteros JA, Gether U. Agonist-induced conformational changes at the cytoplasmic side of TM 6 in the {beta}2 adrenergic receptor mapped by site-selective fluorescent labeling. J Biol Chem. 2000 [Record as supplied by publisher].

Klein-Seetharaman J, Getmanova EV, Loewen MC, Reeves PJ, Khorana HG. NMR spectroscopy in studies of light-induced structural changes in mammalian rhodopsin: applicability of solution (19)F NMR. Proceedings of the National Academy of Sciences of the United States of America. 1999; 96:13744–13749. [PubMed: 10570143]

Knierim B, Hofmann KP, Ernst OP, Hubbell WL. Sequence of late molecular events in the activation of rhodopsin. Proceedings of the National Academy of Sciences of the United States of America. 2007; 104:20290–20295. [PubMed: 18077356]

Kobilka BK. Amino and carboxyl terminal modifications to facilitate the production and purification of a G protein-coupled receptor. Anal Biochem. 1995; 231:269–271. [PubMed: 8678314]

Kofuku Y, Ueda T, Okude J, Shiraishi Y, Kondo K, Maeda M, Tsujishita H, Shimada I. Efficacy of the beta(2)-adrenergic receptor is determined by conformational equilibrium in the transmembrane region. Nat Commun. 2012; 3:1045. [PubMed: 22948827]

Lohse MJ, Maiellaro I, Calebiro D. Kinetics and mechanism of G protein-coupled receptor activation. Current opinion in cell biology. 2014; 27:87–93. [PubMed: 24530699]

Meiboom S, Gill D. Modified Spin-Echo Method for Measuring Nuclear Relaxation Times. Rev Sci Instrum. 1958; 29:688–691.

Moukhametzianov R, Warne T, Edwards PC, Serrano-Vega MJ, Leslie AG, Tate CG, Schertler GF. Two distinct conformations of helix 6 observed in antagonist-bound structures of a beta1-adrenergic receptor. Proceedings of the National Academy of Sciences of the United States of America. 2011; 108:8228–8232. [PubMed: 21540331]

Nygaard R, Zou Y, Dror RO, Mildorf TJ, Arlow DH, Manglik A, Pan AC, Liu CW, Fung JJ, Bokoch MP, et al. The dynamic process of beta(2)-adrenergic receptor activation. Cell. 2013; 152:532–542. [PubMed: 23374348]

Okada T, Ernst OP, Palczewski K, Hofmann KP. Activation of rhodopsin: new insights from structural and biochemical studies. Trends Biochem Sci. 2001; 26:318–324. [PubMed: 11343925]

Parkes JH, Liebman PA. Temperature and pH dependence of the metarhodopsin I-metarhodopsin II kinetics and equilibria in bovine rod disk membrane suspensions. Biochemistry. 1984; 23:5054–5061. [PubMed: 6498176]

Rasmussen SG, Choi HJ, Fung JJ, Pardon E, Casarosa P, Chae PS, Devree BT, Rosenbaum DM, Thian FS, Kobilka TS, et al. Structure of a nanobody-stabilized active state of the beta(2) adrenoceptor. Nature. 2011a; 469:175–180. [PubMed: 21228869]

Rasmussen SG, Choi HJ, Rosenbaum DM, Kobilka TS, Thian FS, Edwards PC, Burghammer M, Ratnala VR, Sanishvili R, Fischetti RF, et al. Crystal structure of the human beta2 adrenergic G-protein-coupled receptor. Nature. 2007; 450:383–387. [PubMed: 17952055]

Rasmussen SG, DeVree BT, Zou Y, Kruse AC, Chung KY, Kobilka TS, Thian FS, Chae PS, Pardon E, Calinski D, et al. Crystal structure of the beta2 adrenergic receptor-Gs protein complex. Nature. 2011b; 477:549–555. [PubMed: 21772288]

Rosenbaum DM, Cherezov V, Hanson MA, Rasmussen SG, Thian FS, Kobilka TS, Choi HJ, Yao XJ, Weis WI, Stevens RC, et al. GPCR engineering yields high-resolution structural insights into beta2-adrenergic receptor function. Science. 2007; 318:1266–1273. [PubMed: 17962519]

Rosenbaum DM, Zhang C, Lyons JA, Holl R, Aragao D, Arlow DH, Rasmussen SG, Choi HJ, Devree BT, Sunahara RK, et al. Structure and function of an irreversible agonist-beta(2) adrenoceptor complex. Nature. 2011; 469:236–240. [PubMed: 21228876]

Sekhar A, Kay LE. NMR paves the way for atomic level descriptions of sparsely populated, transiently formed biomolecular conformers. Proceedings of the National Academy of Sciences of the United States of America. 2013; 110:12867–12874. [PubMed: 23868852]

Shi L, Kay LE. Tracing an allosteric pathway regulating the activity of the HslV protease. Proceedings of the National Academy of Sciences of the United States of America. 2014; 111:2140–2145. [PubMed: 24469799]

Smith SO. Structure and Activation of the Visual Pigment Rhodopsin. Annu Rev Biophys. 2010

Spoerner M, Hozsa C, Poetzl JA, Reiss K, Ganser P, Geyer M, Kalbitzer HR. Conformational states of human rat sarcoma (Ras) protein complexed with its natural ligand GTP and their role for effector interaction and GTP hydrolysis. The Journal of biological chemistry. 2010; 285:39768–39778. [PubMed: 20937837]

Standfuss J, Edwards PC, D'Antona A, Fransen M, Xie G, Oprian DD, Schertler GF. The structural basis of agonist-induced activation in constitutively active rhodopsin. Nature. 2011; 471:656–660. [PubMed: 21389983]

Swaminath G, Xiang Y, Lee TW, Steenhuis J, Parnot C, Kobilka BK. Sequential Binding of Agonists to the {beta}2 Adrenoceptor: Kinetic evidence for intermediate conformational states. J Biol Chem. 2004; 279:686–691. [PubMed: 14559905]

Trzaskowski B, Latek D, Yuan S, Ghoshdastider U, Debinski A, Filipek S. Action of molecular switches in GPCRs--theoretical and experimental studies. Current medicinal chemistry. 2012; 19:1090–1109. [PubMed: 22300046]

Zou Y, Weis WI, Kobilka BK. N-terminal T4 lysozyme fusion facilitates crystallization of a G protein coupled receptor. PLoS One. 2012; 7:e46039. [PubMed: 23056231]

Highlights

- Two inactive states predominate in unliganded and antagonist bound β_2AR
- Agonists increase structural heterogeneity in β_2AR cytoplasmic domains
- The agonist binding pocket and cytoplasmic surface have weak allosteric coupling
- Complete receptor activation requires G protein or a mimetic nanobody

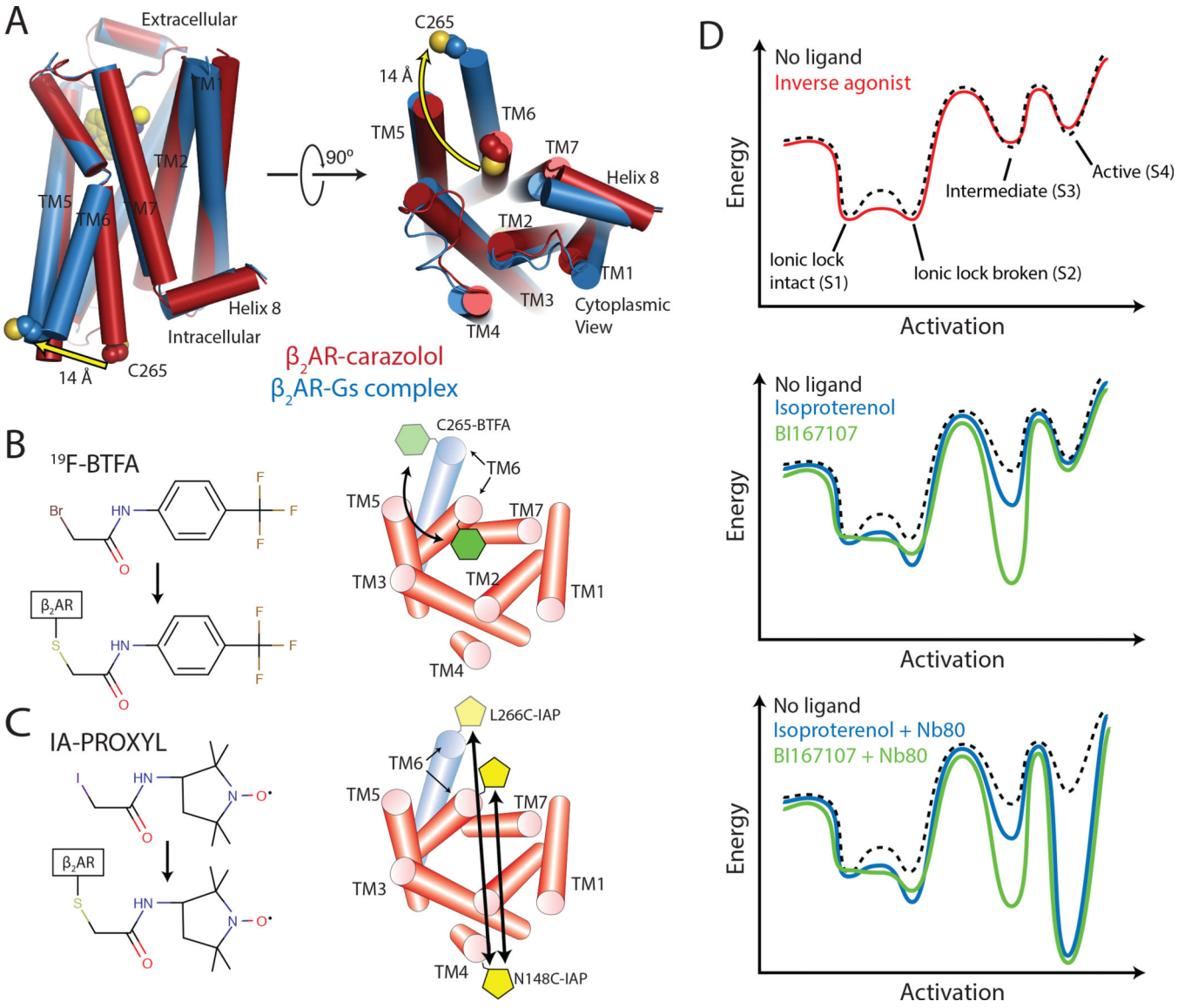

Figure 1.

Spectroscopic methods for detecting conformational changes of β_2AR.

(A) Comparison of crystal structures of inactive, carazolol-bound and active β_2AR in complex with agonist BI167107 and G_s. The crystal structures reveal a 14 Å outward displacement of TM6 upon β_2AR activation. Cys265, used for ^{19}F-NMR experiments is highlighted in spheres.

(B) ^{19}F-NMR studies utilize the fluorine label 2-bromo-4-(trifluoromethyl)acetanilide (^{19}F-BTFA) that reports changes in the chemical environment at the cytoplasmic end of TM6. See Figure S1 and Table S1 for construct design and validation.

(C) For DEER spectroscopy, β_2AR was labeled at the cytoplasmic ends of TM4 (site N148C-IAP) and TM6 (site L266C-IAP) with the nitroxide label 3-(2-iodoacetamido)-2,2,5,5-tetramethylpyrroline-1-oxyl (IA-PROXYL).

(D) Energy landscape of β_2AR in the presence of inverse agonists carazolol and ICI-118,551, agonists isoproterenol and BI167107, and agonists with Nb80.

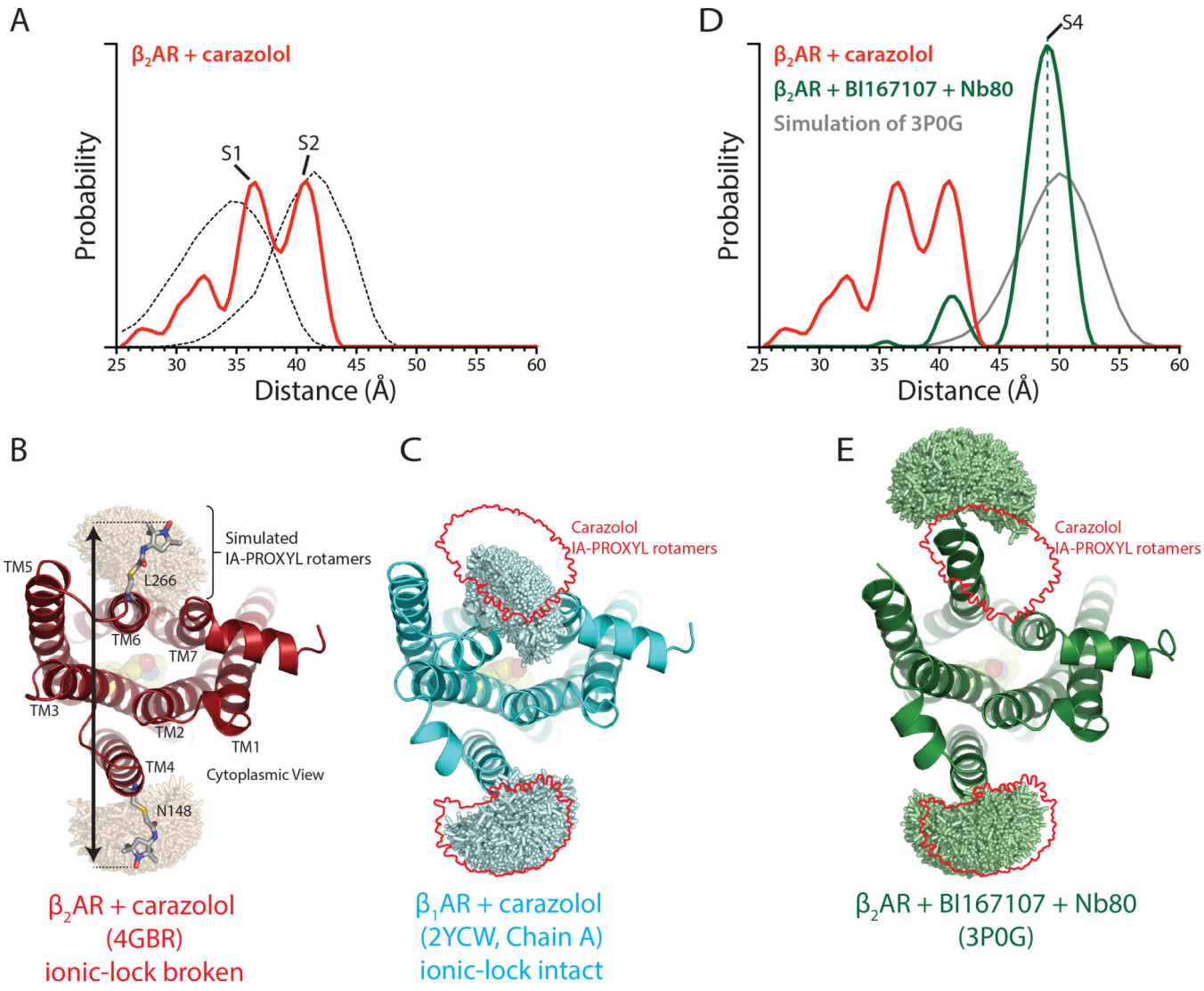

Figure 2.

DEER distances of inactive and fully active β_2AR. See Figure S2 for raw DEER data.

(A) Distance distribution for carazolol-bound β_2AR. The dotted lines show simulated nitroxide spin label distance distributions for a state with a broken ionic lock using carazolol-bound β_2AR (PDB ID: 4GBR), and a state with an ionic lock intact using β_1AR (PDB ID: 2YCW) as shown in panels B and C.

(B) IA-PROXYL rotamers modeled onto β_2AR bound to carazolol (PDB ID: 4GBR) using MTSSLWizard. The distance between these possible rotamers is then determined in a pairwise manner to yield the predicted distance distribution shown in A.

(C) Similar analysis as in B was performed on the structure of β_1AR bound to carazolol but with an intact ionic lock. The red outline indicates rotamers modeled in B. The mean distance for a state with an intact ionic lock is predicted to be shorter than for β_2AR with a broken ionic lock.

(D) Distance distribution for β_2AR bound to BI167107 and Nb80. The dashed green line serves as a marker for the S4 state. The grey line represents the simulated distance

distribution for β_2AR bound to BI167107 and Nb80 using the previously determined crystal structure (PDB ID: 3P0G) as shown in panel E.

(E) IA-PROXYL rotamer modeling of activated β_2AR bound to BI167107 and Nb80.

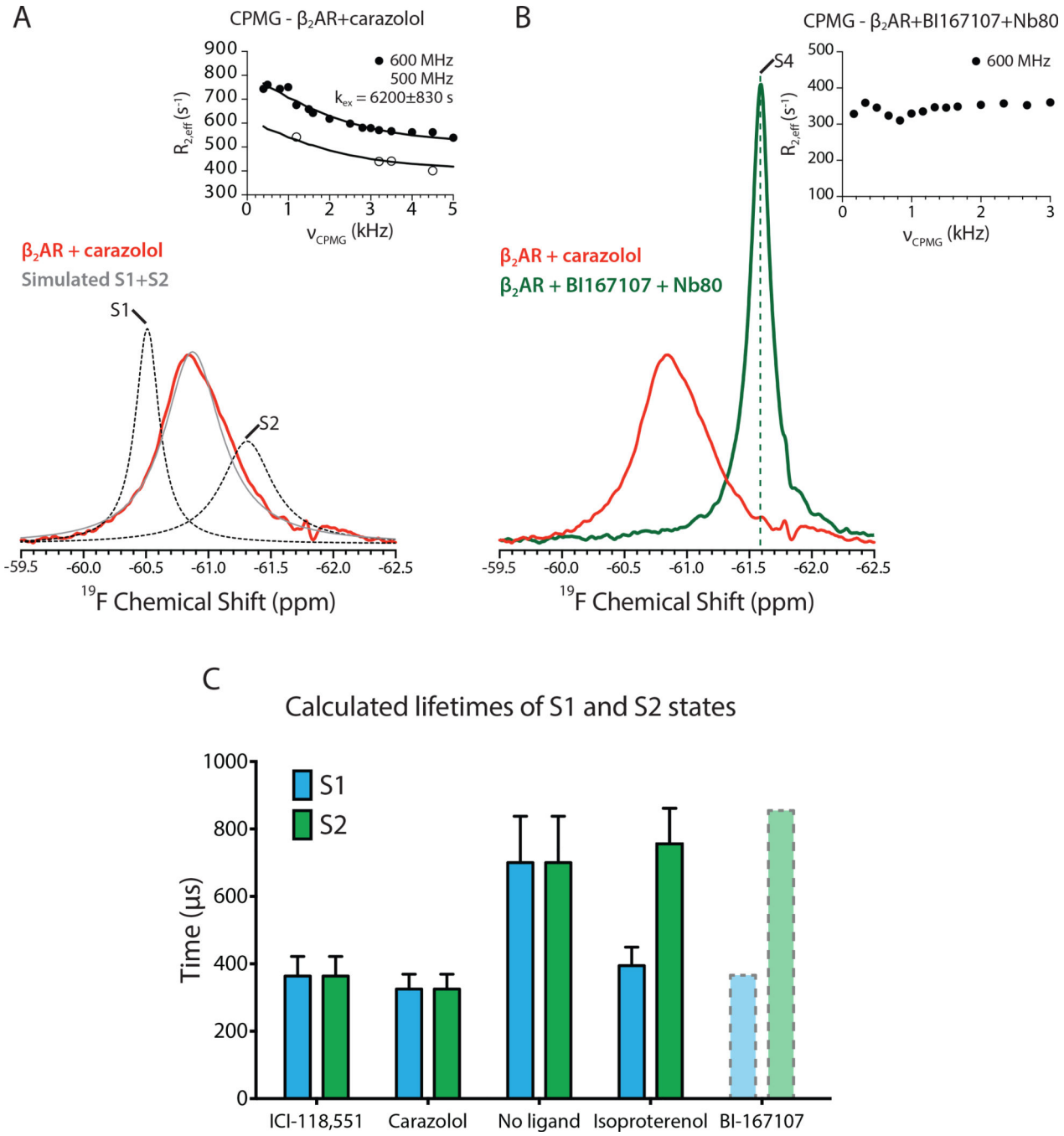

Figure 3.

^{19}F-NMR spectra of inactive and fully active β_2AR. See Figure S3 for raw NMR data. (A) ^{19}F-NMR spectrum of carazolol-bound β_2AR. The inset shows the presence of fast timescale dynamics as assessed by CPMG relaxation dispersion profiles at two magnetic fields (500 MHz and 600 MHz). The simulated S1 and S2 peaks in the absence of exchange are shown in dotted lines and the simulated combined lineshape arising from exchange of S1 and S2 is shown in grey. The simulated lineshapes are further illustrated in Figure S3. The estimated errors in $R_{2,eff}$ for CPMG studies are smaller than the graphics used for

illustration. S tandard errors in k_{ex} are dependent on errors in $R_{2,eff}$, which were estimated by the spectral noise and variation in spectra between experiments from identically prepared samples. See Extended Experimental Methods for more details.

(B) ^{19}F-NMR spectrum of β_2AR bound to BI167107 and Nb80. The dashed green line serves as a marker for the S4 state. Inset shows the absence of CPMG relaxation dispersion for β_2AR bound to BI167107 and Nb80.

(C) Lifetimes of the S1 and S2 states for β_2AR were calculated using the measured exchange rates and the populations estimated by lineshape simulation. As the k_{ex} could not be experimentally determined for β_2AR bound to BI167107, there is potential for error in the simulated populations and lifetimes. The data is therefore illustrated in dotted lines. Error bars represent errors propagated from CPMG fits and determination of S1 and S2 populations. Generally, inverse agonists decrease the lifetime of both the S1 and S2 states, while agonists decrease the lifetime of the S1 state while preserving the lifetime of the S2 state.

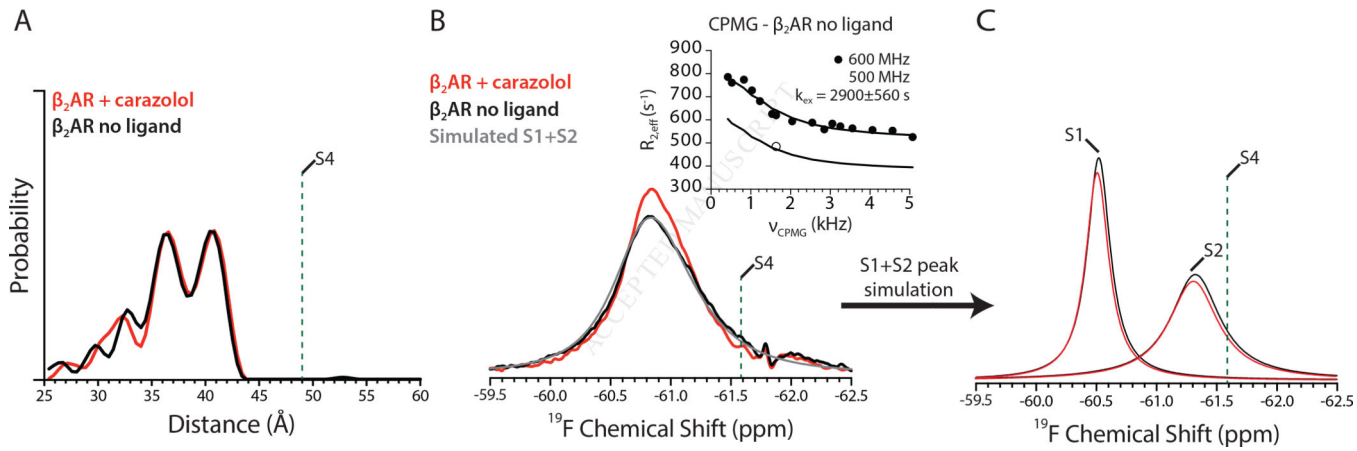

Figure 4.

Spectroscopic insights into basal activity of unliganded β_2AR.

(A) DEER derived distance distributions for unliganded β_2AR with the carazolol-bound distribution superimposed. See Figure S3 for DEER data with ICI-118,551.

(B) ^{19}F-NMR spectra of unliganded β_2AR with CPMG relaxation dispersions shown in the inset. The simulated lineshape for unliganded β_2AR is shown in grey.

(C) ^{19}F-NMR simulated S1 and S2 states for unliganded β_2AR compared to carazolol-bound β_2AR.

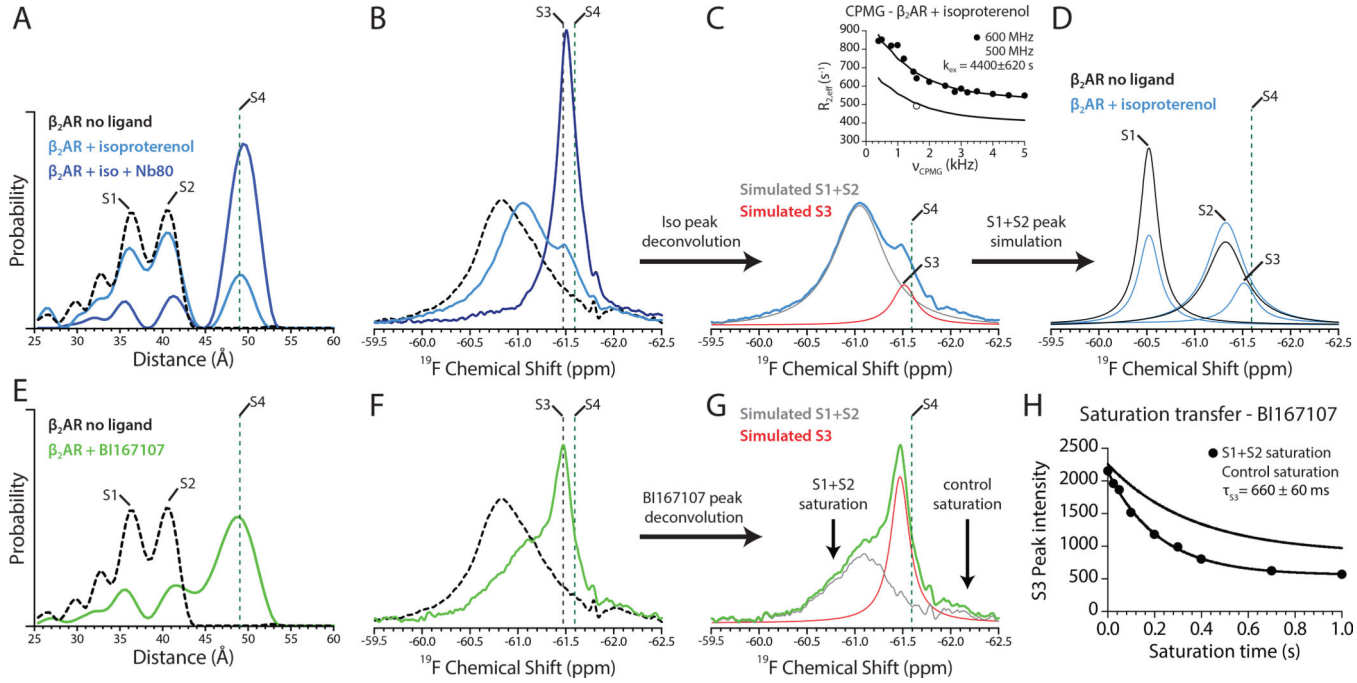

Figure 5.

Agonists induce conformational heterogeneity in the cytoplasmic domain of β_2AR.

(A) Distance distributions for β_2AR in the presence of isoproterenol alone and with Nb80. The dashed black trace represents the distribution from unliganded β_2AR. DEER experiments do not provide sufficient resolution to distinguish S3 from S4.

(B) NMR spectrum of isoproterenol-bound β_2AR shows the presence of a new upfield peak corresponding to S3 (−61.47 ppm) as well as a peak originating from fast exchange of S1 and S2 states. Addition of Nb80 causes a transition to a peak between the S3 and S4 states (−61.51 ppm). The S4 state has a chemical shift of −61.59 ppm. See Figure S5 for isoproterenol lineshape analysis.

(C) Deconvolution of β_2AR+isoproterenol without Nb80 to highlight the S3 state. CPMG dispersion of the S1+S2 peak is shown in the inset.

(D) Simulation of S1 and S2 states for β_2AR bound to isoproterenol and comparison with unliganded β_2AR shows an increase in the S2 state for isoproterenol-bound receptor.

(E) DEER distance distribution for β_2AR bound to BI167107.

(F) ^{19}F-NMR spectrum of β_2AR bound to BI167107, with a new peak at S3 (−61.47 ppm).

(G) Deconvolution of β_2AR+BI167107 spectrum into S1+S2 and S3 peaks. Arrows indicate positions of the spectrum irradiated in saturation transfer experiments with the resulting decay in signal shown in (H). See Figure S5 for saturation transfer NMR spectra.

(A–G) Dashed green lines indicate the conformational signals observed for β_2AR bound to BI167107 and Nb80.

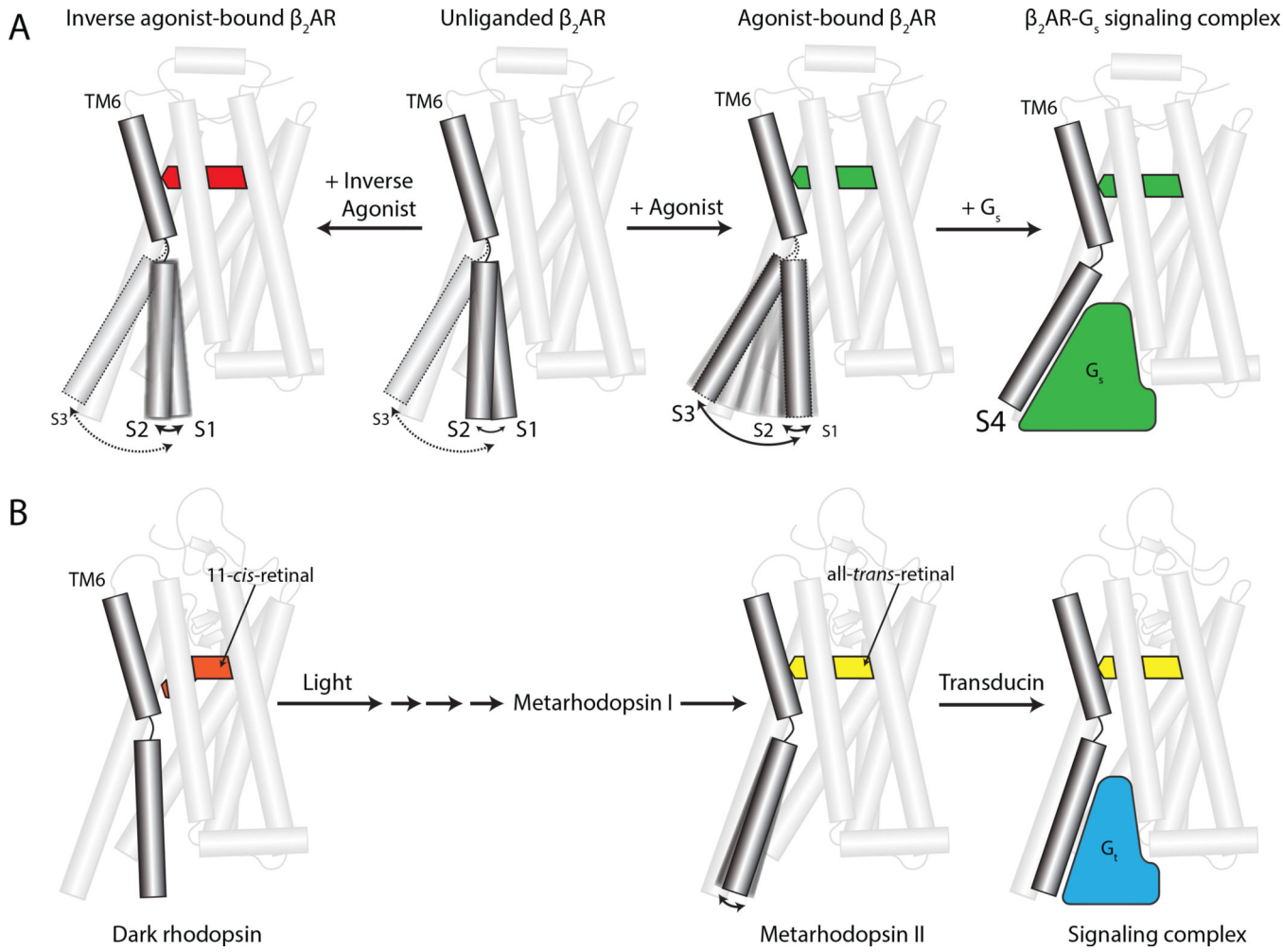

Figure 6.

Differences in the dynamic character of rhodopsin and β_2AR.

(A) The β_2AR is conformationally dynamic in the inactive state, and agonists induce further dynamics to varying degree. The active state is only stabilized in the presence of either G protein or a G protein mimetic. Inverse agonists increase the rate of exchange between ionic lock intact (S1) and broken (S2) states, thereby reducing the lifetime of both states.

(B) Dark rhodopsin is minimally dynamic due to the highly efficacious inverse agonist 11-*cis*-retinal. Illumination by light induces a conformational change to Metarhodopsin II and an accompanying outward displacement of TM6. This active state is then recognized by the G protein transducin (G_t).